Physics (John Wiley & Sons, Inc., New York, 1952). See especially Chap. VI. 3.
[9]A. R. Edmonds, Angular Momentum in Quantum Mechanics (Princeton University Press, Princeton, New Jersey, 1957).
[10]Landolt-Börnstein Numerical Data and Functional Relationships in Science and Technology, edited by K. -H. Hellwege (Springer-Verlag, Berlin, Germany, 1967), New Series, Group 1, Vol. 2, "Nuclear Radii," See Chap. 2 by H. R. Collard and R. Hofstadter.
[11]A. G. C. Cameron, Can. J. Phys. 35, 1021 (1951).
[12]Handbook of Mathematical Functions, edited by M. Abramowitz and I. A. Stegun, National Bureau of Standards, Applied Mathematics Series No. 55 (U. S. Government Printing Office, Washington, D. C., 1964).
[13]E. Hayward, Rev. Mod. Phys. 35, 324 (1963); Nuclear Structure and Electromagnetic Interactions, edited by N. MacDonald (Plenum Press, Inc., New York, 1965).

PHYSICAL REVIEW C VOLUME 1, NUMBER 5 MAY 1970

Pion Elastic Scattering from Carbon and Oxygen at 30 MeV*

J. F. Marshall† and M. E. Nordberg, Jr.‡
University of Rochester, Rochester, New York 14627

and

R. L. Burman§
University of Rochester, Rochester, New York 14627
and Los Alamos Scientific Laboratory, University of California, Los Alamos, New Mexico 87544
(Received 10 November 1969)

Measurements of elastic scattering were made for π^+ and π^- beams at 30 MeV on a carbon target and π^+ on oxygen at 30 MeV. A magnetic spectrometer utilizing wire spark chambers was used to measure the momenta of the scattered pions over the angular range 40–120 deg. The energy resolution was about 4 MeV full width at half maximum at 30 MeV, which is sufficient to resolve the first excited states of carbon and oxygen. Inelastic scattering from the lower excited states has been estimated. Fits of the Kisslinger optical model to the data have been made.

I. INTRODUCTION

There have been theoretical efforts in recent years to produce an optical model of low-energy pion-nucleus scattering from multiple-scattering theory.[1–4] In these calculations it is assumed that off-energy-shell effects can be neglected so that the pion-nuclear interaction can be calculated from free pion-nucleon phase shifts. This approach is motivated by the relatively weak elementary interactions at energies which are low compared with that of the first pion-nucleon resonance. Additional advantages in the theoretical understanding of the pion-nucleus interaction are the lack of identity between the projectile and target nucleons and the relatively small mass and zero spin of the pion.

There are unique aspects of the pion-nucleus interaction which set it apart from those of other nuclear probes. These include single- and double-charge-exchange scattering, the absorption of pions with the subsequent ejection of nucleons or of high-energy γ rays, and the study of pion capture x rays. In the last mentioned case, the study of the complex energy shifts in various Bohr orbits is equivalent to a phase-shift analysis at slightly negative energies.

A fundamental starting point for studying these interactions is the measurement of pion-nuclear elastic scattering. It should be especially interesting to compare the elastic scattering data at small positive energies with the results of pion capture x-ray experiments.

A clear conclusion from the attempts to fit optical models to pion-nucleon elastic scattering is that a nonlocal, or momentum-dependent, optical model is required. The first model of this type which was proposed was the Kisslinger model,[2] which includes a gradient term in the potential.

Another nonlocal optical model has been derived by Ericson and Ericson[3] which applies to pion-nuclear scattering for energies $\lesssim$30 MeV. The potential includes absorption, and has no free parameters. Because of the dominance of the dipole component in πN scattering, short-range nucleon pair correlations are important in the multiple scattering. This produces an effect analogous to the Lorentz-Lorenz effect in the scattering of electromagnetic waves in dense media. The potential of Ericson and Ericson also contains a term which gives a small hyperfine coupling.

Previous measurements of the π^+C elastic cross section were made at this laboratory for pion en-

ergies of 31.5[5] and 40[6] MeV. Fits of the data from those experiments have been made using the Kisslinger model.[4] The complex constants were determined by a search procedure using the values calculated from the elementary interactions as a starting point.

The goal of the present experiment was to extend the measurements of the pion elastic cross section at 30 MeV to the π^-C and π^+O reactions, and to repeat the π^+C measurements with improved statistics and energy resolution.

EXPERIMENTAL PROCEDURE

A low-energy external pion beam at the Rochester synchrocyclotron was produced by bombardment by the 240-MeV internal proton beam of a carbon target in the vacuum tank of the accelerator. The pion beam was then extracted and focused by the fringing field of the main cyclotron magnet and an analyzing magnet. By reversing the cyclotron magnetic field, the analyzing magnetic field, and the sense of circulation of the cyclotron proton beam, the charge of the pion beam is reversed without changing the spatial or momentum distributions of the beam.

In order to reduce the spread of the pion beam in energy and space, a remotely positioned vertical slit 1.5 in. wide was installed upstream of the analyzing magnet entrance as shown in Fig. 1. The resulting beam had a peak energy at the target position of 32 ± 2 MeV and energy spread of 3.0 MeV full width at half maximum (FWHM). The slit reduced the intensity of the beam to 5×10^5 min^{-1} of π^+ and 2×10^5 min^{-1} of π^-.

The peripheral "Cee" electrode was used in the regenerative mode[7] to increase the coarse-structure duty cycle of the cyclotron to better than 90%. A small burst of prompt beam was eliminated by means of an rf gate which cut off the counters for about 5% of the 300-Hz audio frequency cycle at the proper time.

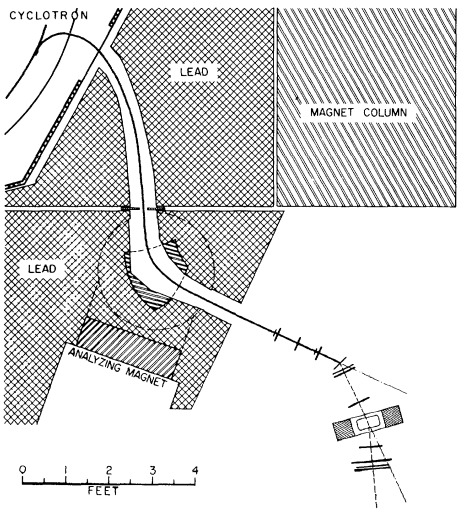

FIG. 1. Pion beam and general experimental arrangement.

A magnetic spectrometer was used to measure the momentum distribution of the particles which emerged from the target. The experimental arrangement is shown in Fig. 2. The beam incident on the target was defined by scintillation counters C1 and C2 and by wire spark chambers SP1, SP2, and SP3. Upon scattering in the target, the scattered pion traversed counter C3, wire spark chambers SP4 and SP5, the magnet, wire spark chambers SP6 and SP7, and finally counters C4 and C5. The trigger logic was $1\,2\,3\,4\,5\,\bar{6}$. The anticoincidence counter, $\bar{C6}$, was placed behind the target to reduce the random trigger rate. The spark chambers had vertical wires with spacing of 0.050 in. Because the magnet gap was only 1.5 in. high, the measurement of the projection of the trajectories on the median plane was adequate for the momentum determination. The magnet gap was 3 in. wide by 6 in. long, and the deflection of the central ray was about 19° for pions of 30-MeV energy. The spectrometer, including its associated counters and spark chambers, was mounted on a rigid aluminum plate equipped with rollers so that the entire assembly pivoted about the target center for setting the angle of scattering. The center of the spectrometer could be rotated through angles from 0 to 120°. The angular resolution was limited by multiple scattering in the target and the counters. All pion momenta greater than 60 MeV/c could be measured. The lower limit was set by the energy required to penetrate the counter and spark chamber arrays.

The wire spark chambers were interfaced to an on-line PDP-8 computer with ferrite-core temporary storage. The "wires" of the spark chambers were made by photoetching thin copper-clad Mylar

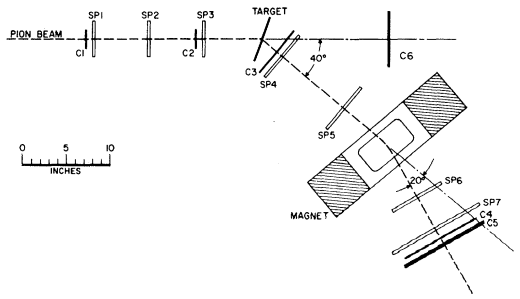

FIG. 2. The wire spark-chamber spectrometer. C1–C6 are scintillation counters. SP1–SP7 are wire spark chambers.

films. The block diagram of the trigger logic and spark chamber read-in system is shown in Fig. 3. Upon receipt of a trigger, the PDP-8 was programmed to sequentially pulse the core drivers of the spark-chamber interface, yielding signals from the sense amplifiers of those cores which had been set by spark currents. From the position of the set cores in the sequence, the spark coordinates were calculated and stored in a memory buffer for later transfer to magnetic tape. The on-line program also displayed plan views of the events on an oscilloscope, and recorded the relative efficiencies of the various spark chambers and the number of times multiple sparks occurred in each chamber. For topologically simple events, the momenta and scattering angles of the events were calculated and typed out. Auxiliary on-line programs were used for measuring direct-beam-momentum spectra and spark-chamber efficiencies.

The carbon scattering was measured with target thicknesses of 0.54 ± 0.02 g cm^{-2} for angles up to 100° in the transmission geometry and 0.223 ± 0.01 g cm^{-2} in the reflection geometry for angles greater than 100°.

The π^+O scattering was measured with a water target. This target was 1.00 ± 0.04 g cm^{-2} in thickness over the beam intersection area, and was used in the transmission geometry only. Since the target was rotated through half the scattering angle, there was a systematic decrease in average scattering energy from the smallest to the largest angle. The shift was 1.5 MeV for the $\pi^{\pm}$C scattering and 2.5 MeV for π^+0. Taking this into account, the mean energy of scattering was 27.8 MeV for π^-C, 30.2 MeV for π^+C and 30.0 MeV for π^+0. The uncertainty in these values was estimated to be ±2.0 MeV.

Because of the low beam intensities, the data of this experiment were taken over a four-month running period. To assure that there were no long-term shifts in the efficiencies, the spectrometer was returned to the direct pion beam about once a week to determine counter and spark-chamber efficiencies. Also the range of angles was spanned

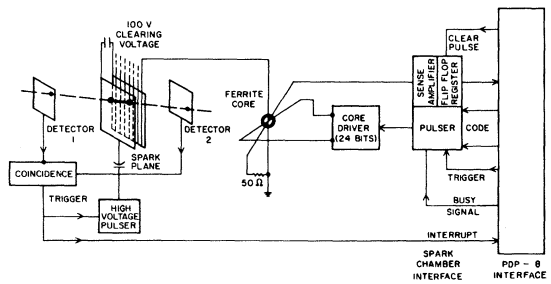

FIG. 3. Block diagram of the wire spark chamber and trigger circuitry.

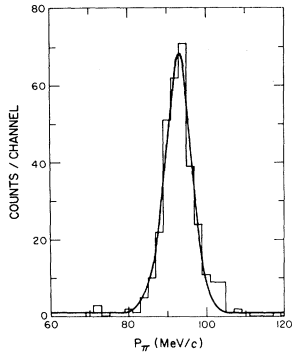

FIG. 4. Fit to the π^- beam spectrum.

at least twice in the course of each measurement of each interaction so that adjacent points were not measured consecutively.

A. Calibration of the Spectrometer

In order to calibrate the spectrometer, the magnetic field of the spectrometer was first mapped with a Gauss meter. Then by means of "hot wire" measurements, pion trajectories were simulated. For the accuracy required for this experiment, about ±3% in momentum, a two-dimensional model of the field with five adjustable constants was found to be an adequate representation. The initial values of the constants were determined from the wire simulated trajectories. Then the spectrometer was placed in the direct pion beam. A range curve of the beam had been measured previously, and the energy distribution of the beam was calculated in terms of the range of the pions in copper, as tabulated by Rich and Madey.[8] By means of an on-line program, which was based on the magnetic field model, the momentum distribution of the measured pion trajectories was calculated and compared with the range-curve measurement. The constants of the model spectrometer were adjusted until the average momentum of the calculated spec-

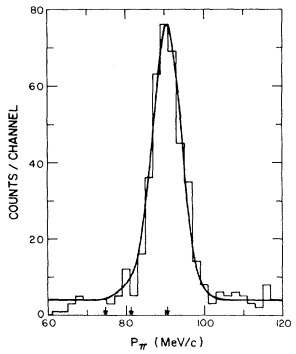

FIG. 5. Fit to a typical carbon-scattered π^+ spectrum. Arrows indicate the momenta of the elastic peak and the first and second excited states.

trum agreed with that deduced from the range-curve measurement and the apparent momentum spread was minimized. As shown in Fig. 4 for the π^- beam, the shape of the momentum spectrum at the center of the spectrum was nearly Gaussian with a rms deviation of 3.35 MeV/c and peak momentum of 92.9 MeV/c. The π^+ beam was similar (Fig. 5), but of slightly higher average momentum. The momentum corresponds to a peak pion energy of 28.1 MeV with ± 1.8-MeV rms deviation. The calibration was checked at different energies spanning the region of interest by inserting absorbers at the target position to degrade the beam.

The principal limitation on momentum resolution was multiple scattering in the spark chambers and intervening air. The effect of multiple scattering was reduced somewhat by installing thin-walled helium channels in the region between the spark chambers. The contribution of the resolution of the spectrometer to the apparent energy spread was estimated to have ± 1.2-MeV rms deviation, with an intrinsic beam width of ± 1.3-MeV rms deviation derived from the range measurements.

B. Particle Identification

The electron contamination in the incident beam was large, but it could be eliminated to within an estimated 2% of the total beam intensity by means of the threshold attenuator settings on the 1 and 2 counters, since the pulse heights of the pions were about twice as great as those of the electrons.

Two procedures were used to measure the direct-beam muon contamination. First there was an apparent high-energy tail on the differential range curve of the beam. This tail was consistent with an (11 ± 2)% fraction of muons with about the same momentum as the pions. The second method was to set the spectrometer into the direct beam, and by placing sufficient absorber between the 4 and 5 counters to stop most of the pions while allowing most of the muons to pass. With this method, the muon intensity was measured to be (9 ± 2)% of the total beam intensity. (The average and relative spread of the muon momentum spectrum were about the same as for the pions.)

In the scattered beam, it was necessary to distinguish the scattered pions from muons, which were produced by the decay of pions in the vicinity of the target, and from protons, which were produced by pion capture in the target. The flux of scattered muons produced by Coulomb scattering of the muons of the direct beam was estimated from the first Born approximation for scattering of muons from uniformly charged spheres.[5]

Muons were produced by the decay of pions downstream from counters 1 and 2. Calculation of the decay kinematics show that the momentum spectrum of muons produced by the decay of 30-MeV pions is strongly peaked at about 65 MeV/c and that the angular distribution is strongly peaked near the maximum decay angle of 22° lab. At the 40- and 50-deg settings, muons which decayed in the vicinity of the target entered the spectrometer aperture. Because of the effects of single and multiple Coulomb scattering in the target, both preceding and following the decay events, the number of muon triggers with the target in the holder was greater than the number measured with the target out. Muon events in all cases were clearly distinguishable from inelastically scattered pions through consideration of the momentum distribution and apparent scattering angle.

Protons were produced by the absorption of pions in the target nuclei. Because of the thickness of counter 4, only protons with momenta greater than 180 MeV/c in the center of the spectrometer were able to produce triggers. Therefore, the minimum detectable proton momentum was 80 MeV/c greater than the maximum expected pion momentum of 100 MeV/c.

C. Analysis

The coordinates of all sparks for events in which two of the three incident-track spark chambers and three of the four scattered-track spark chambers fired were recorded on magnetic tape during the experiment. Events with fewer chambers fired were assumed to be random events. The number of recorded events relative to the number of trigger events was monitored throughout the experimental runs as a measure of the over-all system efficiency.

From the recorded event coordinates, an off-line program was used to reconstruct the tracks of the scattering events. By imposing the constraint that incident and exit tracks must intersect in the target, and must lie on a plausibly continuous track through the magnet, it was possible to eliminate most of the spurious sparks which occurred at a rate of 2–3% of the single-spark rate in each chamber. Also, events in which only one spark chamber failed to fire were recognized by the program, and thus it was possible to deduce the efficiencies of the individual spark chambers and the over-all event efficiency of the system. The resulting individual efficiencies were checked against efficiencies measured with the spectrometer in the direct beam.

The program discriminated strongly against background produced by pion scattering along the beam trajectory, as well as muon decays far from the target region. The apparent true elastic pion

scattering rate with the target out was less than 2% of the rate with the target in and approximately independent of angle. The number of random events obtained from the program agreed well with measured random rates obtained by delaying the incident and scattered counter telescopes by the rf period of the cyclotron, 50 nsec, with respect to the true delay settings.

In order to separate the elastic scattering, the spectra of the scattered pions were fit to three Gaussian peaks plus a constant "background." The fitting function contained 11 free constants which included the positions of the three peaks, their standard deviations, the number of counts in each peak, and the constant background. The constant background was produced by random events, spurious sparks, small-angle rescattering of the pions along the spectrometer trajectory, and pion decays from which the muons passed through the trigger counters. This interpretation was consistent with the number of counts in "forbidden" momentum bands. The momentum-independent background was thrown out. This background was about 5–8% of the elastic scattering rate and approximately independent of angle. The search routine found the minimum of the χ^2 sum in the 11-parameter space. The momentum range of 60–120 MeV/c was divided into 30 bins of 2 MeV/c width and the parameters were varied along the grid of values until the χ^2 sum was stationary with respect to grid variation.

The solid angles were calculated with a ray tracing program to determine the projected acceptance angle of the spectrometer subtended at the target as a function of the target position and pion momentum. The solid angle was corrected for vertical focusing. The calculation of the average projected angular aperture and mean acceptance angle was weighted with the incident beam intensity profile at the target as measured in the incident wire spark chambers. The angular acceptance function of the spectrometer was about 10° FWHM.

D. Corrections and Errors.

Typical corrections and the estimated uncertainties associated with them are listed in Table I. The "relative" column refers to corrections which vary from angle to angle and the "absolute" column is for the part of the correction which relates to the over-all normalization and is the same for every angle. The correction for the muon scattering was obtained from the first Born approximation expression for the scattering from a charged sphere.[5] The correction was important only for the angular range 40–70° lab, where the correction ranged from a factor of 0.970 at 40° to 0.993 at 70°. The method by which the over-all system efficiency was obtained has been described previously. The over-all system efficiency was about 96% for the carbon measurements. During the oxygen run, a failure of the spark chamber read-in system for part of the run required a larger efficiency correction for these data.

The absorption correction was based upon a separate measurement of the total $\pi^{\pm}$C cross section at 30 MeV. The value of 166 ± 30 mb was obtained for the sum of the total absorption cross section and elastic scattering for $\theta \gtrsim 90°$. The procedure was a poor geometry absorption experiment with two scintillation counters for the detection of the pions incident upon a thin carbon target. The fraction of pions which was absorbed was determined by a large third scintillation counter. The experimental uncertainty was large because of the inexact knowledge of the intensity of low-energy particles in the beam which could simulate stopped pions. The water absorption was estimated by multiplying the carbon total cross section by the $\frac{2}{3}$ power of the ratio of the atomic numbers.

The pion-decay corrections were angle dependent because the momenta of the pions emerging from the target depended upon the target orientation. The measured momenta at the center of the spectrometer were used for the calculation. It was assumed that any pion which decayed at any point along the trajectory was lost because of the program requirements on the trajectories. The correction for pion-proton scattering in the hydrogen component of the water target was calculated using a measurement of the π^+p cross section at 31.5 MeV.[9] The method for estimating the intensity of

TABLE I. Typical corrections and their estimated uncertainties.

	$\pi^{\pm}$C		π^{+}O	
	Relative	Absolute	Relative	Absolute
Muon scattering	1.000 ± 0.005	1.000 ± 0.005	1.000 ± 0.005	1.000 ± 0.005
Spark-chamber efficiency	1.040 ± 0.010	1.040 ± 0.010	1.20 ± 0.04	1.40 ± 0.08
Absorption	1.000 ± 0.00	1.002 ± 0.000	1.009 ± 0.002	1.009 ± 0.004
Pion decay	1.000 ± 0.01	1.260 ± 0.026	1.000 ± 0.002	1.265 ± 0.027
Proton scattering			0.974 ± 0.002	1.000 ± 0.002
Incident muons	1.000 ± 0.000	1.10 ± 0.02	1.00 ± 0.00	1.10 ± 0.02

TABLE II. Typical errors (fractional).

	$\pi^{\pm}$C		π^{+}O	
	Relative	Absolute	Relative	Absolute
Effective target thickness	0.01	0.04	0.02	0.08
Counting losses	0.00	0.02	0.00	0.02
Random events	0.00	0.02	0.00	0.02
Beam muons	0.00	0.01	0.00	0.01
Solid angle	0.02	0.05	0.02	0.05
Fitting	0.03	0.05	0.03	0.05
Statistical	0.08	0.08	0.08	0.08
Beam electrons	0.00	0.02	0.00	0.02
Beam protons	0.00	0.00	0.00	0.00
Background subtraction	0.00	0.01	0.00	0.01

muons in the incident beam was described previously.

Typical values of the estimated errors are listed in Table II. "Relative" error means the angle-to-angle error, and "absolute" error refers to the part of the cross-section normalization error which is common to all the angles. Of these, only the fitting and statistical errors are random errors. The rest are estimates of the systematic errors. Typically, the statistical errors were somewhat larger than the sum of the systematic errors.

III. RESULTS

The data for the elastic scattering cross sections have been listed in Table III. The normalization is experimental, with a factor 1.00 ± 0.12 for $\pi^{\pm}$C and 1.00 ± 0.14 for π^{+}O. The errors are relative and were obtained by combining the statistical and fitting errors quadratically with the estimated systematic errors. The measurements of the inelastic scattering cross sections were not very precise, because of the small number of inelastic events. The scattering from the 4.43-MeV state of C was approximately isotropic for both π^{+} and π^{-}, with average cross-section magnitudes of 0.40 ± 0.16 mb/sr and 0.52 ± 0.22 mb/sr, respectively. The scattering from the 7.6- and 9.6-MeV states, which was combined by the fitting routine, was about half that from the 4.43-MeV state, although the experimental cutoff at 17 MeV makes this only a rough estimate. The combined scattering from the 6-MeV states of O was also isotropic over the angular range measured in this experiment, and the average cross-section was 0.62 ± 0.07 sm/sr.

The cross section for the production of at least one detectable proton was also isotropic within the experimental error for both π^{+}C and π^{+}O. The average was 2.5 ± 0.4 mb/sr for π^{+}C and 7.3 ± 1.0 mb/sr for π^{+}O.

A. Optical-Model Calculations.

The elastic scattering data were compared to optical-model calculations performed with the ABACUS-M code of Auerbach and Sternheim.[4,10] This optical-model code solves an approximate Klein-Gordon equation with a Kisslinger-model potential,[2]

$$U \propto b_0 p_0^2 \rho - b_1 \vec{\nabla} \cdot (\rho \vec{\nabla}),$$

where ρ is the nuclear density, p_0 the incident pion momentum, and b_0 and b_1 are parameters proportional to pion-nucleon amplitudes. The second term troduces a velocity dependence into the potential which represents the p-wave character of low-energy pion-nucleon scattering. A modified Gaussian function,

$$\rho(r) = \rho_0[1 + (Z - z)r^2/3a^2]e^{-r^2/a^2}$$

was used for both the nuclear density and the charge density.

With the charge-density parameter at $a = 1.66$, variations were made in the nuclear-density parameter, a, and the potential parameters, b_0 and b_1, in order to determine a combined best fit for the $\pi^{\pm}$ scattering on carbon. The results are shown as solid curves in Figs. 6 and 7 for the parameter values: $a = 1.61$, $\mathrm{Re}b_0 = -3.64$, $\mathrm{Im}b_0 = 0.14$, $\mathrm{Re}b_1 = 5.52$, $\mathrm{Im}b_1 = 0.18$. These values are in reasonable agreement with predictions[4] based upon pion-nucleon amplitudes. Over-all, the fits to the data obtained with the Kisslinger-model potential are quite good. It is apparent that the main structure present in the measurement, the different shapes of the nuclear-Coulomb interference region in the $\pi^{\pm}$ scattering, is reproduced by the calculations.

Further, it should be noted that the fit to the π^{+}C scattering could be considerably improved by a 20% decrease in the relative π^{+} to π^{-} experimental normalization; such a decrease would be within our estimated absolute accuracies of ±12%.

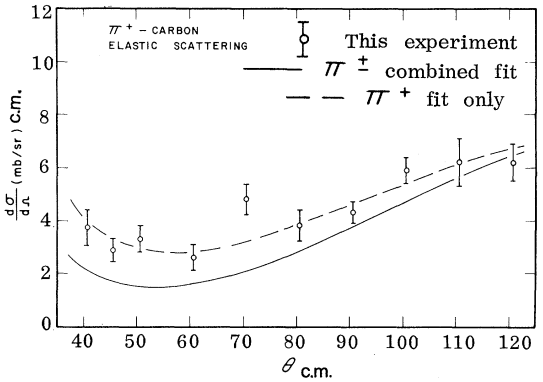

FIG. 6. Kisslinger optical-model fits to the π^+C elastic scattering cross-section data at 30.2 MeV. The solid line is the prediction of the combined $\pi^\pm$ fit and the dashed line is from the fit to the π^+ data only.

The combined fits to the elastic $\pi^\pm$C data have normalized values of $\chi^2 = 7.2$. By allowing the potential parameters b_0 and b_1 to be varied separately for the two cases, it was possible to find better individual fits to the data. These individual fits are shown as the dashed curves in Figs. 6 and 7.

Only the real parts of the potential parameters b_0 and b_1 changed significantly in the individual fits. The parameter values were $\mathrm{Re}b_0 = -4.41$ and $\mathrm{Re}b_1 = 5.26$ for π^+ on carbon, and $\mathrm{Re}b_0 = -3.36$ and $\mathrm{Re}b_1 = 5.68$ for π^- on carbon. Normalized χ^2 values were 1.4 and 5.0, respectively.

Similar optical-model calculations were made for the π^+O elastic scattering data. The Kisslinger-model prediction, with the same potential parameters found for the $\pi^\pm$C combined fit, and with density parameters $a = 1.77$ and $a_c = 1.83$, is shown as a solid curve in Fig. 8. The fit is fair, with a normalized χ^2 of 14. Again, by varying the real parts of the potential parameters, a very good fit with a χ^2 value of 1.2 was obtained, as shown in Fig. 8 by the dashed curve; the new values of the potential parameters were $\mathrm{Re}b_0 = -4.07$ and $\mathrm{Re}b_1 = 4.94$.

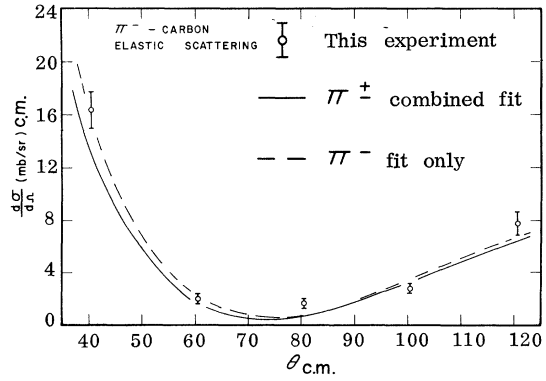

FIG. 7. Kisslinger optical-model fits to the π^-C elastic scattering cross-section data at 27.8 MeV. The solid line is the prediction of the combined $\pi^\pm$ fit, and the dashed line is from the fit to the π^- data only.

It is apparent from a comparison of the data points and the solid curves in Figs. 6–8 that the Kisslinger-model optical potential provides a reasonable description of the elastic scattering of 30-MeV pions from carbon and oxygen. Furthermore, small changes in the real parts of the optical-potential parameters lead to quantitatively accurate fits to the data as shown by the dashed curves in Figs. 6–8. Such changes perhaps reflect a different environment for positive and negative pions. The separate fits to the elastic scattering from carbon require the real parts of the potential parameters to decrease for π^+ scattering and to increase for π^- scattering; this is what might be expected for a smaller effective kinetic energy for π^+ than for π^-, due to the Coulomb potential. However, in view of the near equivalence in the number of data points and number of parameters for the separate fits, the numerical values of the changes in the potential parameters are probably not significant.

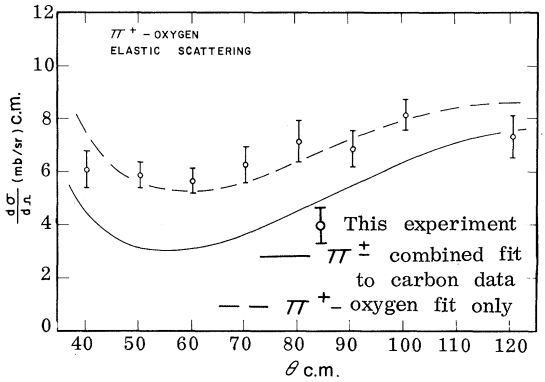

FIG. 8. Kisslinger optical-model prediction and the π^+O elastic scattering data. The solid curve was obtained by using the parameters b_0 and b_1 from the combined $\pi^\pm$C data. The dashed curve was obtained by fitting the π^+O data only.

TABLE III. The pion-nucleus elastic cross sections are given in mb.

Lab angle (deg)	π^+C	π^-C	π^+O
40	3.62 ± 0.68	16.0 ± 1.29	5.96 ± 0.72
45	2.78 ± 0.40	•••	•••
50	3.29 ± 0.46	•••	5.81 ± 0.51
60	2.56 ± 0.43	2.02 ± 0.36	5.62 ± 0.54
70	4.78 ± 0.52	•••	6.21 ± 0.66
80	3.85 ± 0.52	1.64 ± 0.25	7.21 ± 0.78
90	4.31 ± 0.36	•••	6.86 ± 0.71
100	6.00 ± 0.50	2.68 ± 0.29	8.24 ± 0.58
110	6.35 ± 0.80	•••	•••
120	6.41 ± 0.67	7.89 ± 0.90	7.50 ± 0.83

B. SUMMARY AND DISCUSSION

The results of the optical-model calculations from this work and from the work of Auerbach, Fleming, and Sternheim[4] are summarized in Table IV. The theoretical values of the optical-model parameters were calculated by Auerbach, Fleming, and Sternheim from phenomenological pion-nucleon phase shifts. They pointed out that the largest theoretical uncertainty is associated with $\mathrm{Re}b_0$ which is quite sensitive at low momenta to slight deviations from the free pion-nucleon amplitudes. It is clear that the largest difference between the fitted parameters and the theoretical parameters is for $\mathrm{Re}b_0$. Also the calculated imaginary parts of both b_0 and b_1 are lower than the expected values. It should be noted that Auerbach, Fleming, and Sternheim expected good agreement between theory and experiment for the Kisslinger model only for a small energy region around 80 MeV.

The agreement between the results of this experiment and the data of Kane[5] for π^+C is good both for the elastic cross section as shown by the parameters listed in Table IV, and for the proton-production and inelastic data.

Further analysis taking into account the effective kinetic energy of the pion inside the nucleus, the Lorentz-Lorenz effect or short-range nucleon-nucleon correlations, and pion capture should clarify the reason for the apparent difference in the calculated optical-model parameters for π^+ and π^-.

In summary, it can be said that the Kisslinger model provides a reasonably good representation of low-energy pion-nuclear elastic scattering. This model should provide a good starting point for the analysis of the large quantities of precise pion-nuclear data which will undoubtedly be available within a few years as improved meson facilities are brought into operation.

TABLE IV. Summary of the results of the optical-model calculations.

b_0	b_1	Source
$-3.64+0.14i$	$5.52+0.18i$	combined $\pi^{\pm}C$ fit
$-4.41+1.14i$	$5.26+0.18i$	π^+C fit only (30.2 MeV)
$-3.36+0.14i$	$5.68+0.18i$	π^-C fit only (27.8 MeV)
$-4.07+0.14i$	$4.94+0.18i$	$\pi^{\pm}0$ fit only (30.0 MeV)
$-3.71+0.13i$	$5.90+0.16i$	π^+C fit to Kane's data (31.5 MeV)[a]
$-0.50+0.53i$	$6.30+0.40i$	π^+C theory (31.5 MeV)[a]

[a]See Ref. 4.

ACKNOWLEDGMENTS

The authors wish to acknowledge the assistance of Professor M. M. Sternheim who made the ABACUS-M optical-model code available.

Also we wish to express our appreciation to Professor E. H. Thorndike for encouragement and valuable advice.

Finally, the experiment would not have been possible without the able assistance of the staff of the cyclotron laboratory in the design and fabrication of apparatus, and without the patience of the cyclotron operating crew during the long hours of running required by the experiment.

---

*Work partially conducted under the auspices of the U. S. Atomic Energy Commission.

†Present address: Xerox Corporation, Rochester, New York 14603.

‡Present address: Wilson Synchrotron Laboratory, Cornell University, Ithaca, New York 14850.

§Present address: Los Alamos Scientific Laboratory, Los Alamos, New Mexico 87544.

[1]K. M. Watson, Rev. Mod. Phys. 30, 565 (1958).

[2]L. S. Kisslinger, Phys. Rev. 98, 761 (1955).

[3]M. Ericson and T. Ericson, Ann. Phys. (N.Y.) 36, 323 (1966).

[4]E. H. Auerbach, D. M. Fleming, and M. M. Sternheim, Phys. Rev. 162, 1683 (1967).

[5]P. P. Kane, Phys. Rev. 112, 1337 (1958).

[6]J. Perry, PhD. thesis, University of Rochester, 1953 (unpublished).

[7]E. Nordberg, IEEE Trans. Nucl. Sci. NS-12, 973 (1965).

[8]M. Rich and R. Madey, University of California Radiation Laboratory Report No. UCRL-2301, 1954(unpublished).

[9]C. W. Barnes, B. Rose, G. Giacomelli, J. Ring, K. Miyake, and K. Kinsey, Phys. Rev. 117, 276 (1960).

[10]E. H. Auerbach and M. M. Sternheim, Brookhaven National Laboratory Report No. 12696, 1968 (unpublished).

[11]E. H. Auerbach, H. M. Qureshi, and M. M. Sternheim, Phys. Rev. Letters 21, 162 (1968) and references therein.